ALEPH 92-132
PHYSIC 92-121
S. Snow and S. Adlung
4.8.1992

Tau Polarization in the Electron Channel

Stephen W. Snow
Lancaster University
Sönke Adlung
MPI Munich

31 July 1992

Abstract

The tau polarisation is measured using the electronic decay mode for the 1990 and 1991 data separately. The method is essentially based on the one used for the tau polarisation paper. The combined result of both years, avaraged over the polar angle, is P=$(-12.7 \pm 10.3_{stat} \pm 5.5_{sys})$%. In addition a measurement of the polarisation as a function of the polar angle is performed. Under the assumption of lepton universality this analysis yields P=$(-17.4 \pm 8.8_{stat} \pm 3.9_{sys})$%.

1 Introduction

A main task in the selection of electrons coming from τ decays is the rejection of background coming from Bhabha events. In order not to be hampered by its large amount at small scattering angles the electron part of the published analysis on τ polarization [1] was restricted to the barrel region ($|cos\theta| < 0.7$).

The present analysis of the 1990 and 1991 data is based on a selection procedure very similar to the previous one. But it makes full use of the detector, the polar angle of the jets being extended to $|cos\theta| < 0.9$ as for the other τ decay channels.

Including the endcaps we have essentially two reasons to use the ECAL pad energies instead of the wire energies for the polarization fit:

- *Leakage:* The loss of energy in the material before the active region of ECAL is much greater in the endcaps than in the barrel. A suitable leakage correction is automatically applied by JULIA to the clusters, but not to the wire energies.
- *Non-uniformity:* There is a variation of response with the position of the shower in some modules. In the endcaps the main effect is due to different capacitance in different parts of the module, which effects only the wire energies, not the pad energies.

2 Summary of Cuts

1. *Event Pre-Selection*
   a) A good track is defined as a track with $|d_0| < 2cm, |z_0| < 10cm, TPChits > 3, |cos\theta| < 0.95, p > 0.1GeV$. At least one good track per hemisphere is required. The total number of good tracks must be greater than 1 and less than 7, with at least one of them having $p > 3GeV$. In case of more than 4 good tracks, the

opening angle of each jet must have $cos\eta > 0.85$. These criteria are slightly more stringent than the common lepton selection class 15.

b) The acolinearity angle between the two jet axes is required to be greater than $(\pi - 0.25)rad.$

c) The total transverse momentum with respect to the beam axis in at least one of the two hemispheres must be greater than 2GeV.

d) The HV bit of ECAL must be on for every selected event.

e) Every ECAL module hit by one of the good tracks must produce a wire energy of at least $10MeV$.

2. *Electron Definition*

a) 1 good track with $ITChits > 3, TPChits > 4, |cos\theta| < 0.9, p > 2GeV$.

b) No "bad track" ($2cm < |d_0| < 20cm, |z_0| < 20cm, TPChits > 3, p > 0.1, |cos\theta| <$ 0.95) within $1rad$ of the good track.

c) The electron estimators from the EIDT bank must be available and they are restricted to $-2.5 < R2$ and $-2.5 < R3 < 3.0$.

d) A dE/dx estimator $R5$ is formed with QDEDXM if there are signals available. In this case it must be greater than -2.5. For $p < 5GeV$ it *must* be available with signals from at least 80 wires.

e) The number of hit planes in HCAL must be less than 3.

3. *ECAL Fiducial*

The curved track is extrapolated into ECAL using AUHCYL from the ALEPHlib. The region codes of the ECAL geometry are taken from the JULIA routine EBCDRG.

a) The track must not hit an ECAL crack or overlap region.

b) The tangent to the track at the origin must not extrapolate to an ECAL crack or overlap.

4. *Opposite Hemisphere*

a) The fastest track in the hemisphere opposite to the electron candidate must pass the ECAL fiducial cuts or the number of hit HCAL planes in this hemisphere must be greater than 10.

b) The fastest track must not be an electron (based on $R2, R3, dE/dx$, i.e. 2.c and 2.d).

c) The total energy in the opposite hemisphere, measured with ECAL wires, must be less than 75% of the beam energy.

This set of cuts provides a sample of electrons with very low background from other τ decay channels. The background from non tau events is mainly Bhabhas and is strongly peaked at $X_e = 1$. There is also a small background from two photon events. The main differences compared to the previous analysis [1] are:

- The extension to the endcap regions.
- A more efficient way to distinguish between cracks and sensitive regions of ECAL.
- The use of a wider road in HCAL resulting in a more efficient rejection of hadronic τ decays.
- The acceptance of a fraction of those events with a μ or π on the recoil side even if it passes through an ECAL crack or overlap region.

3 Results

The overall efficiency as a function of the electron energy is shown in figure 1. It is almost flat in the region $0.1 < X_e < 0.9$ which is used for the polarization fit. The mean value in this energy range is $43.7 \pm 0.3\%$ for 1990 and $42.8 \pm 0.3\%$ for 1991.Figure 2 shows the background from other τ decay channels. It is mainly from the ρ and $a1$ channel and tends to be at the higher X region. It is due to events in which the photons of the π_0 overlap with the impact point of the charged track into ECAL to give a shower which looks like an electron. In the fit range this background is always less than 4% of the electron signal and on average it is $(0.41 \pm 0.05)\%$ in 1990 and $(0.72 \pm 0.07)\%$ in 1991.

When this analysis is applied to the data it finds 1172 electrons in 1990 and 2050 electrons in 1991. We use "perfect" and "maybe" runs at all LEP energies. The measured electron spectrum of ECAL pad energies is then fitted to a mixture of Monte Carlo events generated with positive and negative helicity. The MC contains the small fraction of background from misidentified τ decays in a very similar distribution in energy that is found in the data (cf. section 4.2). The background of two electron events (including the case where both taus decay into an electron) has been estimated from real data events as well (cf. section 4.3). In the fit range it amounts to $(2.2 \pm 0.5)\%$ in 1990 and $(1.9 \pm 0.3)\%$ in 1991. This background is included in the fit. Taking into account the different overall efficiencies derived from the two MC samples of fixed helicity, the ratio of the mixture provides the measured τ polarization. The fit region is restricted to the energy range $0.1 < X_e < 0.9$. The first bin has been excluded because of the bad ECAL response at low energies. The bins with $X_e > 0.9$ have been excluded because of the increased amount of Bhabha background in this region. Details of the fitting procedure are decribed in the appendix.

Figure 3 and 4 show the fit results before any systematic corrections. The uncorrected polarizations are measured to $P_{\tau^-} = (-37.3 \pm 18.0_{stat} \pm 4.8_{MCstat})\%$ in 1990 and $P_{\tau^-} = (-1.8 \pm 12.6_{stat} \pm 4.5_{MCstat})\%$ in 1991. The χ^2 of these fits are 1.1 and 2.0 respectively.

4 Systematics

The systematic errors can be divided into two contributions. A first contribution due to all uncertainties which are in some way directly related to the particular choice of the set of cuts. A second contribution due to those uncertainties which are expected to be independent of the choice of the cuts. The latter consists of systematic errors in the fitting procedure, caused by uncertainties in the ECAL energy scale (cf. section 4.4) and the finite statistics of the two MC samples used to fit the data (cf. appendix). The first contribution is the one which requires some more sophisticated procedures in order to be measured:

The overall efficiency of the cuts can be devided into:

- The acceptance caused by track quality cuts, event topology cuts and geometrical cuts. Since the efficiency of track reconstruction, the topology of tau events and the geometry of ALEPH are very accurately decribed by the simulation programs their contribution to the systematic errors can be ignored.

- The efficiency of the particle identification.
  - If the electron identification efficiency has a different energy dependence in real data and Monte Carlo the fit will be biased. The systematic corrections and uncertainties of this bias are estimated in section 4.1.
  - The background from misidentified tau decays depends on the same subset of cuts. An estimate of the amount of this background in the data compared to the MC and its influence on the fit result are discussed in section 4.2.
- The efficiency of the cuts against two electron events. The use of cuts in the opposite hemisphere has the advantage that the amount of this background in the selected set of $\tau \rightarrow e\nu_e\nu_\tau$ candidates can be measured directly from the data. This measurement and the resulting systematic error on the polarization are discussed in section 4.3.

4.1 Electron Identification Efficiency

4.1.1 The ECAL Cuts

The electron identification efficiency as a function of the energy can be measured using e^+e^- pairs from Bhabha events and from photon conversions in hadronic events. These events are tagged by the identification of one of the electrons and the efficiency is determined as the probability to identify the other.

In case of Bhabha events there must be one hemisphere with 1 track, $X > 0.9$ and $R2 > -2.5$. In addition the missing mass of the whole event must be less than 1 GeV. This selection provides a test sample of electrons in the second hemisphere which is used to measure the efficiencies of the ECAL cuts $R2$ and $R3$ for energies $X > 0.8$. For these energies the MC predicts that there is virtually no background from τ events in the selected electron sample.

Candidates of e^+e^- pairs from photon conversions are found with the ALEPHlib routine PAIRFD. The photon is assumed to come from the interaction point and the angle between its momentum and the momentum of the tracks outgoing from the materialization point must be less than 18°. The two tracks under consideration must have an invariant mass of less than $20MeV$ and a minimal distance in the x-y-plane of less than $4mm$. One track must be identified to be an electron ($-2.5 < R2, -2.5 < R3 < 3, -2.5 < R5$). To avoid overlapping of clusters, the entrance point of the second track into the ECAL must have a minimal distance to the cluster of the first track of $15cm$. The distance in the x-y-plane between the materialization point of the photon and the interaction point must be between 3 and $16cm$ or between 26 and $37cm$. Figure 5 shows these distances for the selected pair candidates. We take only those pairs which are produced in the region of either the VDET or the outer ITC and inner TPC boundary. According to the MC this selection provides an electron test sample with $(2.8 \pm 0.3)\%$ background in 1990 and $(3.6 \pm 0.3)\%$ background in 1991. The backgound is mainly π and its distribution in energy is very similar to that of the electrons (fig.5). Assuming the same background distribution to be present in the data test sample as well, its influence on the efficiency corrections will be completetly negligible.

Figure 6 and 7 show the efficiency of the ECAL cuts ($R2, R3$) as a function of the

measured pad energy for real data and MC events. A straight line is fitted to the ratio of both efficiencies. The fitted parameters provide an efficiency correction which must be applied to the MC spectra. The sigma of the slope propagates into a systematic uncertainty of the polarization. The corrections are $\Delta P = +2.5 \pm 1.1$ in 1990 and $\Delta P = -1 \pm 0.7$ in 1991.

Though the helicity fit is performed only in the region $0.1 < X_e < 0.9$, the next and second next bin are included in the straight line fit to the ratio of the efficiencies. This has been done in order to include the region which is populated by "typical" Bhabha events, assuming that actually there should not be a large fluctuation between adjacent bins.

There is a problem with the momentum distribution in the 1990 Bhabha MC. Figure 8 shows these distributions for MC and data in the selected Bhabha test sample. It can be seen that the MC distribution is shifted to higher momenta by roughly +2%. Presumably this is due to an unsufficient simulation of radiative corrections in the Bhabha generator used for the 1990 MC. Though there is not perfect agreement in 1991, the MC of that year much better reproduces the data distribution.

Figure 9 shows the $R2$ distributions in 1990 on both sides of the Bhabha peak ($0.8 < X_e < 1$ and $1 < X_e < 1.2$). In the high energy part the $R2$ distributions are centered around positive values, in the low energy part around negative values. Since we cut at $R2 > -2.5$, the discrepancy between data and MC has a significant influence on the efficiencies in the low energy part, whereas those in the high energy part are hardly influenced by this cut.

Our conclusion is that we can be confident in the efficiencies in the bins above $X_e = 1$ but must be suspicious in the region $0.8 < X_e < 1$. Following this we enlarged the error bars of the ratio eff(data)/eff(MC) of 1990 (fig.6) in the 9th and 10th bin by a factor of 10 to make them have a negligible influence on the straight line fit and the resulting efficiency corrections.

4.1.2 The dE/dx Cut

Figure 10 shows the distribution of the dE/dx estimator for electron candidates which have passed all selection cuts. It can be seen that the peak in the data is narrower than the one in the MC. We estimate the influence on the polarization by a variation of the cut at -2.5 (2.d). In 1991, this cut is placed at 2.71 standard deviations from the mean in the real data and at 2.51 standard deviations in the MC. So we varied the cut position in the real data distribution between -2.5 and -2.3 with the cut in the MC being left unchanged. The resulting correction for the polarization result is $+1.7 \pm 1.2\%$. For 1990, this procedure gives $-0.2 \pm 0.3\%$.

4.2 Background from Other Tau Decay Channels

The background of misidentified τ decays can be estimated by fitting the distribution of the dE/dx estimator. Figure 11 and 12 show these distributions in different energy

ranges before the cut at -2.5 was made. The data is the points with the error bars and the Monte Carlo is the histogram. The Monte Carlo has been devided into events which are known to be electrons (plain) and those which are known to be background (shaded). The relative normalization of electrons and background is the only free parameter of the fit to the data. Using this normalization and the fraction of the shaded histogram which is above the cut at -2.5 we can estimate the background in a way which is not strongly reliant on the Monte Carlo. The result of this estimate, compared with the direct prediction of the Monte Carlo is shown in figure 13. From this figure we conclude that the Monte Carlo correctly predicts the hadronic background in the electron channel to better than $\pm 50\%$. Performing this background variation in the Monte Carlo spectra we estimate a systematic uncertainty on the polarization result of $\pm 1.2\%$ in 1990 and $\pm 2.2\%$ in 1991.

4.3 Non-Tau Background

4.3.1 Background from Well Measured Electron Pairs

If an electron candidate passes all of the cuts except 4.b then its energy is recorded (figure 14). It can be seen that there is a spike at low X_e corresponding to two photon events, a typical $\tau \rightarrow e\nu_e\nu_\tau$ spectrum due to events where both taus decay to an electron, and a Bhabha peak at 1. If the event is not subject to any bias (see below) then we can use the known identification efficiency for normal electrons ($\epsilon_{e(2.c,2.d)} = 94.2\%$) to calculate the background from electron pairs which passed cut 4.b because one electron was not identified. The suitable rescaling of the histogram in figure 14 is done with the factor

$$1.3 \frac{(1-\epsilon_e)}{\epsilon_e}.$$

In principle each event identified as containing two electrons should have entered the histogram twice, but because of the slightly different cut situation on the signal and recoil side of such an event this is not entirely true. For example a high energy electron of the signal side will be rejected when looked at as a recoil electron due to cut 4.c. The factor 1.3 has been introduced in order to take into account that about 70% of the electrons in figure 14 enter this histogram in couples and 30% as singles.

The type of background measured this way is the one which dominates the low X part of the shaded histograms in figure 3 and 4.

4.3.2 Extra Background from Pathological Bhabhas

The method decribed in the previous section does not work for the background where the recoil electron is close to the beam energy. This Bhabha background ought to be removed by cut 4.c. But if it gets past cut 4.c it means there must be something "pathological" about the event. For example the recoil track appears to point to a sensitive region of ECAL but in fact a major fraction of the energy was deposited in a crack between mod-

ules. Under those conditions the identification efficiency of the recoil track will be some unknown number, much less than 94.2%.

The background of this type is estimated by assuming that the energy measurement on the signal side is independent of whether or not there are problems on the recoil side. So we take the energy distribution of well-measured Bhabha electrons (i.e. events which pass all cuts except 4.b *and* 4.c; figure 15) and normalize it to fit the events with $X > 1.0$ in our $\tau \rightarrow e\nu_e\nu_\tau$ candidate spectrum. This is a region where the Monte Carlo predicts that there will be virtually no real $\tau \rightarrow e\nu_e\nu_\tau$ events. This procedure, combined with the background from well-measured electron pairs, gives the shaded region in figure 3 and 4.

We divide the shaded histogram in figure 3 and 4 in two parts, above and below $X_e = 0.8$. Both parts have been varied separately in order to estimate the systematic error due to Bhabha background and two photon background. A variation of the high X part by $\pm 40\%$ in 1990 and $\pm 30\%$ in 1991 corresponds to the statistical error of the background events above $X = 1$. For the low X part the statistical error of the well measured two electron background including the uncertainty of the rescaling factor requires a variation of $\pm 30\%$ in 1990 and $\pm 20\%$ in 1991. The resulting systematic uncertainties on the polarization are $\pm 0.6\%$ and $\pm 0.2\%$ due to Bhabha background and $\pm 0.5\%$ and $\pm 0.3\%$ due to two photon background in 1990 and 1991 respectively.

4.4 ECAL Energy Scale

Throughout this analysis all ECAL energies are corrected for the saturation effect which exists in the data but is not simulated in the Monte Carlo [2]. This effect was measured in test beam data and is described by one parameter:

$$E_{measured} = E_{true}\,(1 - \alpha\, E_{true})$$

where $\alpha = 0.0009$.

All JULIA and ALPHA corrections to ECAL clustering algorithms are applied. In this context we are not hampered by the confusion caused in the 1991 real data reprocessing. The clustering corrections for data and MC in barrel and endcaps are performed with exactly those factors that have been presented in [3].

The measured pad energy is always the total electromagnetic energy of all ECAL objects within a cone of 60° around the jet axis of the corresponding hemisphere.

Barrel and endcaps are calibrated separately to allign E_{pad}/E_{beam} at 1 for *on peak* Bhabha events (figure 16). In addition we included a calibration shift of +3% for the endcap pad energies of the 1990 τ Monte Carlo produced on the IBM of the Rutherford-Appleton Laboratory [4].

We assume an uncertainty in the ECAL energy scale of $\pm 0.5\%$ in the high X part and $\pm 1.3\%$ in the low X part. This values are based on an investigation performed with electrons from Bhabha events and two photon events [3]. Due to less statistics, the low X uncertainty for 1990 is $\pm 2.0\%$. Between the two regions we interpolate with a $1/\sqrt{X}$ dependence. These uncertainties propagate into a systematic error in the polarization of $\pm 2.8\%$ in 1990 and $\pm 4.2\%$ in 1991.

5 Summary and Final Result

Table 1 summarizes the systematic errors and final polarization results for 1990 and 1991. The systematic errors are added in quadrature.

For the combined result of both years we take the weighted avarage with respect to the full statistical error (from both data and Monte Carlo). The same avaraging is applied line by line to obtain the combined systematic errors. The final result is

$$P = (-12.7 \pm 10.3_{stat} \pm 5.5_{sys})\%.$$

Table 1
Summary of Polarization Analysis

Systematic	1990	1991	90+91
ECAL Acc.	$+2.5\% \pm 1.1\%$	$-1.1\% \pm 0.7\%$	$\pm 0.8\%$
dE/dx Acc.	$-0.2\% \pm 0.3\%$	$+1.7\% \pm 1.2\%$	$\pm 0.9\%$
ECAL Scale	$\pm 2.8\%$	$\pm 4.2\%$	$\pm 3.7\%$
Tau Bkg.	$\pm 1.2\%$	$\pm 2.2\%$	$\pm 1.9\%$
Bhabha Bkg.	$\pm 0.6\%$	$\pm 0.2\%$	$\pm 0.3\%$
2 Photon Bkg.	$\pm 0.5\%$	$\pm 0.3\%$	$\pm 0.4\%$
MC Statistic	$\pm 4.8\%$	$\pm 4.5\%$	$\pm 3.4\%$
Total Syst.	$\pm 5.9\%$	$\pm 6.7\%$	$\pm 5.5\%$
Polarization	$(-35.0 \pm 18.0_{stat})\%$	$(-1.2 \pm 12.6_{stat})\%$	$(-12.7 \pm 10.3_{stat})\%$

6 Comparison with Other Analyses

Meanwhile the electron channel has been investigated in the context of complete polarization analyses based on the main 1-prong decay channels ($\tau \to e\nu_e\nu_\tau$, $\tau \to \mu\nu_\mu\nu_\tau$, $\tau \to \pi\nu_\tau$, $\tau \to \rho\nu_\tau$) by groups from the University of Wisconsin [8] and Ecole Polytechnique [9]. A comparison has been presented in the ALEPH tau meeting [10]. Since then some results have been updated for the 1992 Rochester Conference in Dallas [11], [12]. A comparison with most recent numbers is given in table 2.

Table 2
Comparison of Results (90+91)

Systematic	UW	EP	this analysis
Acceptance	$\pm 0.7\%$	$\pm 1.0\%$	$\pm 1.2\%$
ECAL Scale	$\pm 3.4\%$	$\pm 2.8\%$	$\pm 3.7\%$
Tau Bkg.	$\pm 1.4\%$	$\pm 1.6\%$	$\pm 1.9\%$
Non-Tau Bkg.	$\pm 1.6\%$	$\pm 1.2\%$	$\pm 0.5\%$
MC Statistic	$\pm 3.0\%$	$\pm 2.1\%$	$\pm 3.4\%$
Total Syst.	$\pm 5.2\%$	$\pm 4.1\%$	$\pm 5.5\%$
Polarization	$(-31.3 \pm 9.1_{stat})\%$	$(-16.1 \pm 8.9_{stat})\%$	$(-12.7 \pm 10.3_{stat})\%$

The analyses mainly differ in the following points:

- *Run and event selections:* UW and EP use the runs selected by the electroweak group whereas we use all perfect and maybe runs. The event selection of UW is based on a neural network.
- *Handling of cracks and overlaps:* We use different crack and overlap cuts from EP. No such cuts are used by UW.
- *X range of the helicity fit:* UW uses the range $[0,1]$, EP uses the range $[0.1,1]$, whereas we use $[0.1,0.9]$.
- *ECAL pad/wire energies:* EP measures the energy with ECAL wires, while UW and our analysis use the pads.

We expect part of the difference in the final result to be due to the different X fit ranges. For instance including in our analysis the bin $[0,0.1]$ gives a polarization value of -16.2% instead of -12.7%.

7 Polarization vs. Polar Angle

With the combined data of 1990 and 1991 we performed a measurement of the polarization as a function of the polar angle θ. The main features of this kind of analyses are described for the pion decay channel in [5]. We use the same $cos\theta$ binning as for the pion: the data is divided into nine bins, the MC into three bins corresponding to barrel, overlaps and endcaps. The MC binning is also used for the efficiency corrections. For the non-tau background estimations we use 6 bins taking into account the forward-backward asymmetry of the Bhabha events.

In each $cos\theta$ bin the analysis is performed exactly as described in the previous sections. Table 3 summarizes the fit results in each of the $cos\theta$ bins, including the efficiency corrections. Figure 17 shows the fit of the function

$$P(cos\theta) = \frac{P_\tau + P_Z \frac{2cos\theta}{1+cos^2\theta}}{1 + P_\tau P_Z \frac{2cos\theta}{1+cos^2\theta}}$$

under the assumption of lepton universality, i.e. $P_\tau = P_Z = P$. The polarization asymmetry is measured to $P = (-17.4 \pm 8.8_{stat})\%$, the χ^2 of the fit being 1.3.

Table 3
Polarization vs. Polar Angle

$cos\theta$	Real Data Bin (#e)	MC+ Acc. Bin	ee Bkg. Bin	Fit Result %	$\frac{\chi^2}{d.o.f.}$	Total ee Bkg.
-0.9						
	D1 (184)	A1	B1	$-3.9 \pm 52.2_{stat}$	0.7	7.5%
-0.8						
	D2 (286)	A2	B2	$-15.5 \pm 37.1_{stat}$	0.7	6.4%
-0.63						
	D3 (468)	A3	B3	$+4.1 \pm 24.8_{stat}$	1.1	2.2%
-0.4						
	D4 (425)	A3	B3	$+53.7 \pm 23.3_{stat}$	0.7	2.4%
-0.15						
	D5 (489)	A3	B3	$+7.7 \pm 24.1_{stat}$	1.6	2.1%
+0.15						
	D6 (443)	A3	B3	$-40.0 \pm 27.8_{stat}$	0.4	2.3%
+0.4						
	D7 (452)	A3	B4	$-33.7 \pm 27.4_{stat}$	1.2	2.5%
+0.63						
	D8 (297)	A2	B5	$-71.1 \pm 39.5_{stat}$	1.8	7.4%
+0.8						
	D9 (178)	A1	B6	$-86.9 \pm 59.8_{stat}$	1.7	8.6%
+0.9						

The systematics due to MC statistic, ECAL acceptance and non-tau background have been reevaluated in each of the real data bins (table 4). The other systematics are taken from the overall analysis. The reevaluated systematics are assumed to be uncorrelated as long as their estimation is based on different electron samples, i.e. if the real data bins are covered by different acceptance or background bins. For example the systematics due to the ECAL acceptance corrections in bin D1 and D2 are uncorrelated since their measurement was performed with different electron test samples A1 and A2, whereas those of D3 and D4 are correlated.

Table 4
Polar Angle Dependence of Systematics

Data Bin	MC Stat.	ECAL Acc.	ee Bkg.
D1	±11.5%	±2.2%	±2.0%
D2	±8.4%	±1.4%	±0.7%
D3	±3.7%	±0.7%	±0.4%
D4	±3.6%	±0.6%	±0.4%
D5	±3.7%	±0.6%	±0.4%
D6	±4.2%	±0.8%	±0.6%
D7	±4.1%	±0.7%	±0.6%
D8	±10.5%	±1.6%	±1.0%
D9	±16.1%	±1.7%	±2.6%

All uncorrelated systematics are propagated separately into the fit result of figure 17. Their contributions to the uncertainty on P are added in quadrature. Table 5 summarizes the different systematics.

Table 5
Systematics of Polar Angle Analysis

MC Stat.	EC Acc.	ee Bkg.	dE/dx	Tau Bkg.	EC Scale	Σ
±2.5%	±0.5%	±0.3%	±0.7%	±1.3%	±2.5%	±3.9%

The final result of this method is

$$P = (-17.4 \pm 8.8_{stat} \pm 3.9_{sys})\%,$$

showing that there is a worthwhile gain in both statistical and systematic errors when the polar angle information is included.

Appendix: The Fitting Procedure

With $X = E_{pad}/E_{beam}$ we divide the range $0 < X < 1.2$ into 12 bins of equal width. From the real data we have the distribution of selected electron candidates $D(i)$, $i = 1, 12$. In addition, according to the methods described in section 4.3, we estimate which fraction of $D(i)$ to consider as background $B(i)$ from 2 electron events. From the MC we have two spectra $M^+(i)$ and $M^-(i)$ with positive and negative helicity respectively. With

$$D = \sum_i D(i), \quad B = \sum_i B(i), \quad M^+ = \sum_i M^+(i), \quad M^- = \sum_i M^-(i)$$

we use

$$M(i;f) = B(i) + (D - B)\left[f\frac{M^+(i)}{M^+} + (1-f)\frac{M^-(i)}{M^-}\right]$$

and minimize

$$\chi^2(f) = \sum_i \left(\frac{D(i) - M(i;f)}{\sigma(i)}\right)^2$$

with respect to f. The resulting f_{min} could be called "polarization of the τ sample *after* all cuts selecting $\tau \to e\nu\bar{\nu}$ events". However, due to cuts on energy or momentum (like 1.c or 2.a), the overall efficiencies ϵ^+ and ϵ^- are different for the two helicity states. In fact from the MC we can estimate $\epsilon^+ = 37.5\%, \epsilon^- = 41.2\%$ in 1990 and $\epsilon^+ = 37.4\%, \epsilon^- = 40.2\%$ in 1991. The measured τ polarization P is defined as

$$P = \frac{\sigma^+ - \sigma^-}{\sigma^+ + \sigma^-} = \frac{N^+ - N^-}{N^+ + N^-}.$$

With the efficiencies ϵ^+ and ϵ^- from the MC we have

$$N^+ \propto \frac{f_{min}}{\epsilon^+}, \quad N^- \propto \frac{1 - f_{min}}{\epsilon^-}$$

which finally provides P.

An investigation about the "best" choice of the $\sigma(i)$ shows that this choice may significantly influence the polarization result (absolute shifts by a few percent). We follow the conclusions presented in [6] : Instead of using the Poisson errors of the data spectrum, i.e. $\sqrt{D(i)}$, we use those of the theoretically predicted fit function, i.e. $\sigma_{fit}(i) = \sqrt{M(i;f)}$. This has the advantage that a downward fluctuation in the data does not lead to a smaller error which exaggerates the effect of the fluctuation [7]. In addition we have the contribution of the MC statistical error:

$$\sigma^2_{MC}(i) = (D - B)^2 \left[\left(\frac{f}{M^+}\right)^2 M^+(i) + \left(\frac{1-f}{M^-}\right)^2 M^-(i)\right]$$

We perform two χ^2 fits for each year: a first one with $\sigma(i) = \sigma_{fit}(i)$ and a second one with $\sigma^2(i) = \sigma^2_{fit}(i) + \sigma^2_{MC}(i)$. The central value of the polarization is the result of the 2nd fit. As statistical error of this result we quote the error of the first fit. The "systematic" error due to limited MC statistics is calculated as quadratic difference of the errors of the 2nd and the 1st fit.

References

[1] D. Decamp *et al.*, *Measurement of the Polarization of τ Leptons Produced in Z Decays*, Phys.Lett.B **265** (1991) 430

[2] D. Decamp *et al.*, *ALEPH: A Detector for Electron- Positron Annihilations at LEP*, Nucl. Inst. and Meth. in Phys. Res. **A294** (1990) 121-178

[3] M.-N. Minard, Presentation at the ALEPH Tuesday Meeting, 5 May 1992

[4] J. Conway *et al.*, Presentation at the ALEPH Tau Meeting, 3 June 1992

[5] S.W. Snow, *An Update of the Tau Polarization in the Pion Channel*, ALEPH 92-13, Feb. 1992

[6] S.W. Snow, Presentation at the ALEPH Tau Meeting, 23 June 1992

[7] Especially if there are several bins with low population and correspondingly small errors the effect of downward fluctuations is that the fitted curve will be pulled below the avarage value of the data. This problem, for instance, had occured when the Z line shape fits were first being done in 1990 with small sets of data samples at many different points of energy.

[8] J. Conway *et al.*, *Tau and Electron Couplings to the Z from Measurement of the Tau Polarization in ALEPH*, ALEPH 92-77, 1 June 1992

[9] J.C. Brient *et al.*, *τ Polarization in Z Decays. Measurement of the Z to e's and τ's Vector to Axial Coupling Ratios.* ALEPH 92-113, 15 July 1992

[10] J.C. Brient, Presentation at the ALEPH Tau Meeting, 23 June 1992

[11] H.Videau *et al.*, Presentation at the ALEPH Tuesday Meeting, 23 July 1992

[12] M.Schmitt *et al.*, Presentation at the ALEPH Tuesday Meeting, 23 July 1992

Figure 1 : The overall efficiency of the selection program as a function of the true electron energy $X_e = E_{true}/E_{beam}$ according to the MC.

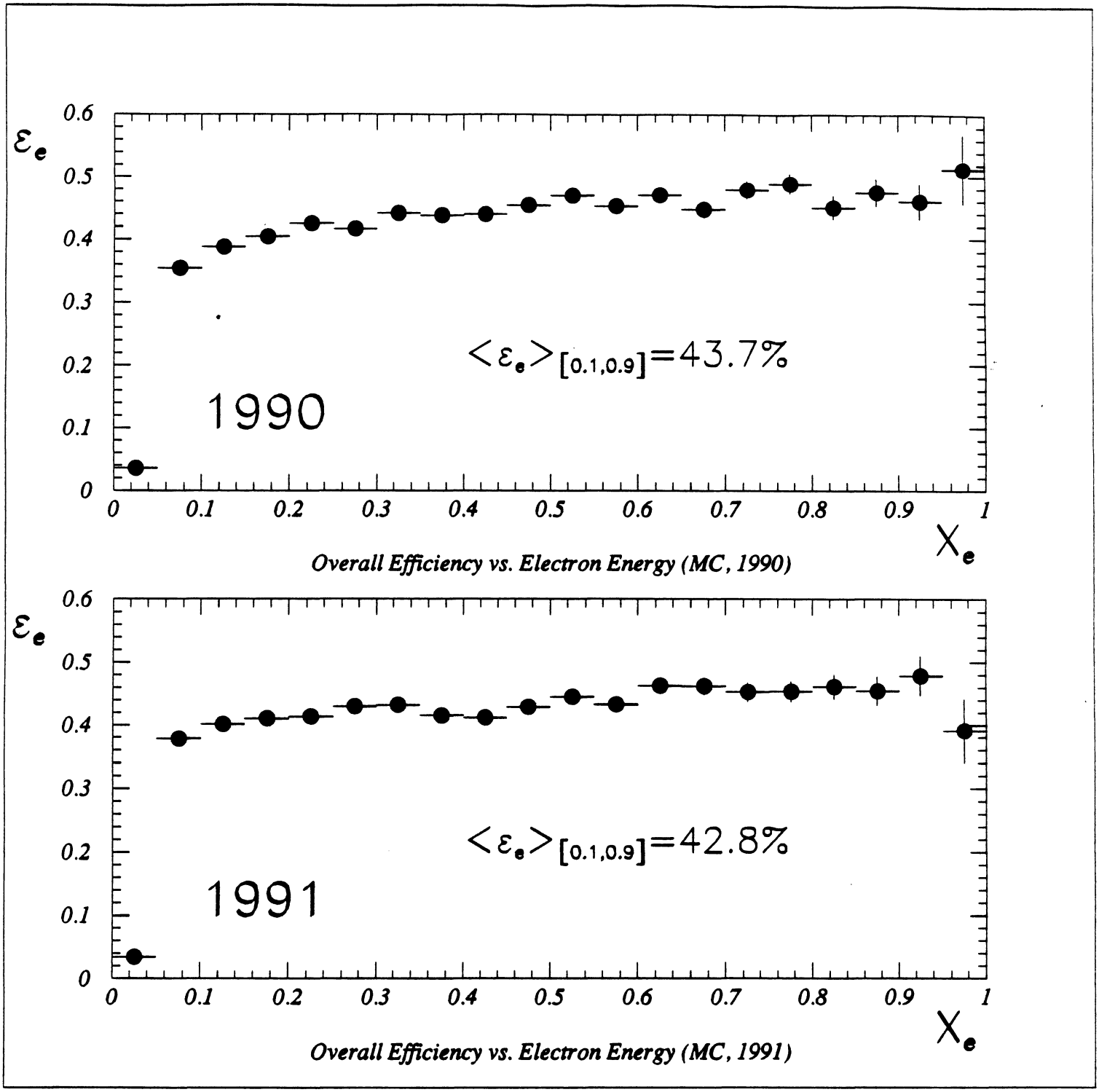

Figure 2 : The background from other τ decay channels as a function of the measured ECAL pad energy $X_e = E_{pad}/E_{beam}$ according to the MC.

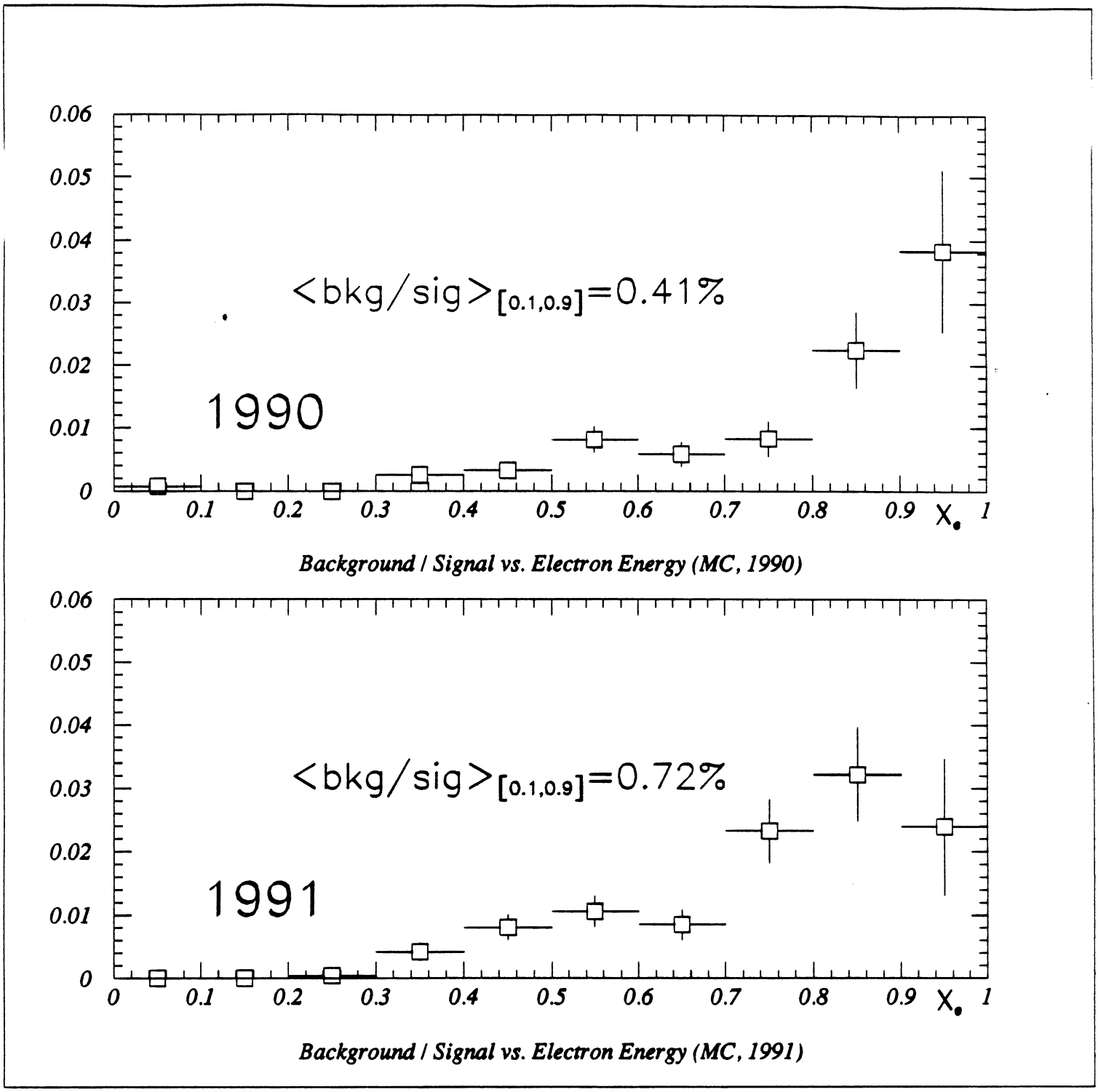

Figure 3 : The helicity fit for the data taken in 1990. Without any systematic corrections the fit result is

$$P = (-37.3 \pm 18.0_{stat} \pm 4.8_{MCstat})\%, \quad \chi^2 = 1.1$$

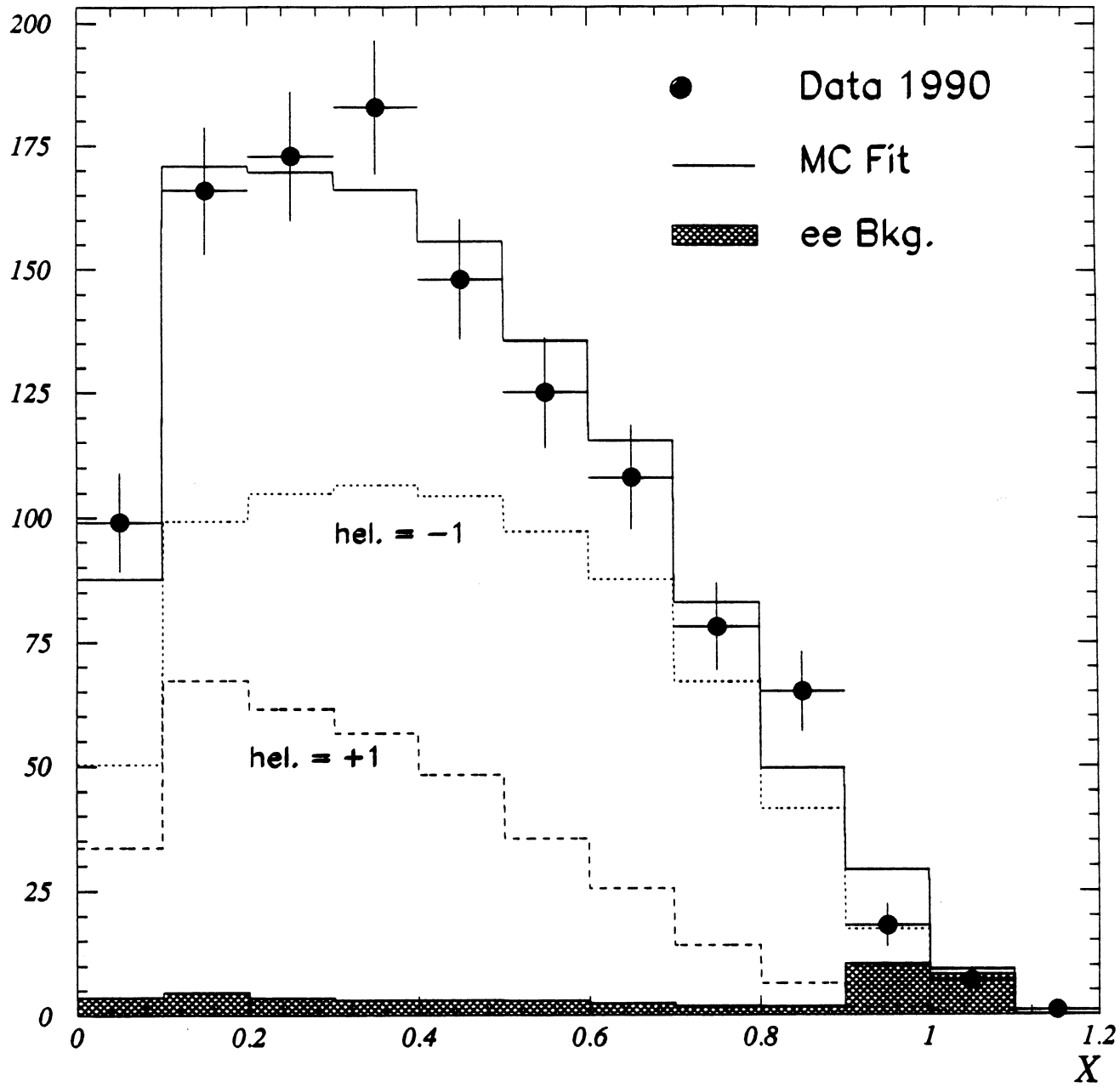

ECAL pad spectrum for selected electron candidates (1990)

Figure 4 : The helicity fit for the data taken in 1991. Without any systematic corrections the fit result is

$$P = (-1.8 \pm 12.6_{stat} \pm 4.5_{MCstat})\%, \quad \chi^2 = 2.0$$

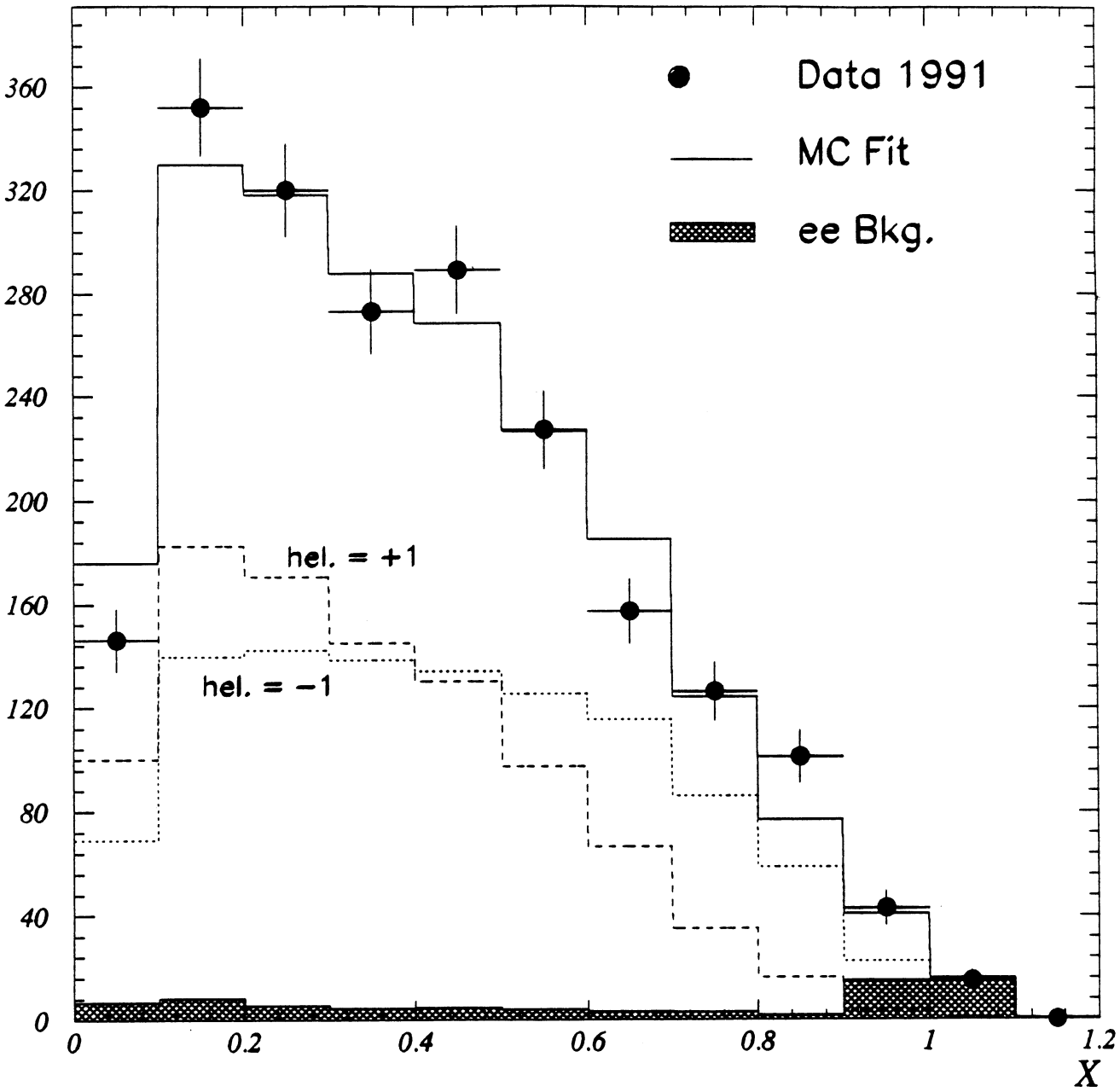

ECAL pad spectrum for selected electron candidates (1991)

Figure 5 : Selection of the electron test sample from photon conversions in hadronic events: The first two plots show the distribution of the conversion radius in the xy plane. The data is the points with error bars, the MC is the histogram. The distributions are normalized to the number of hadronic events. Part of the discrepancy in 1990 could be due to a generator problem; in addition the amount of VDET radiation length was underestimated. The third plot shows the ECAL pad energies of electrons and background in the selected MC test sample.

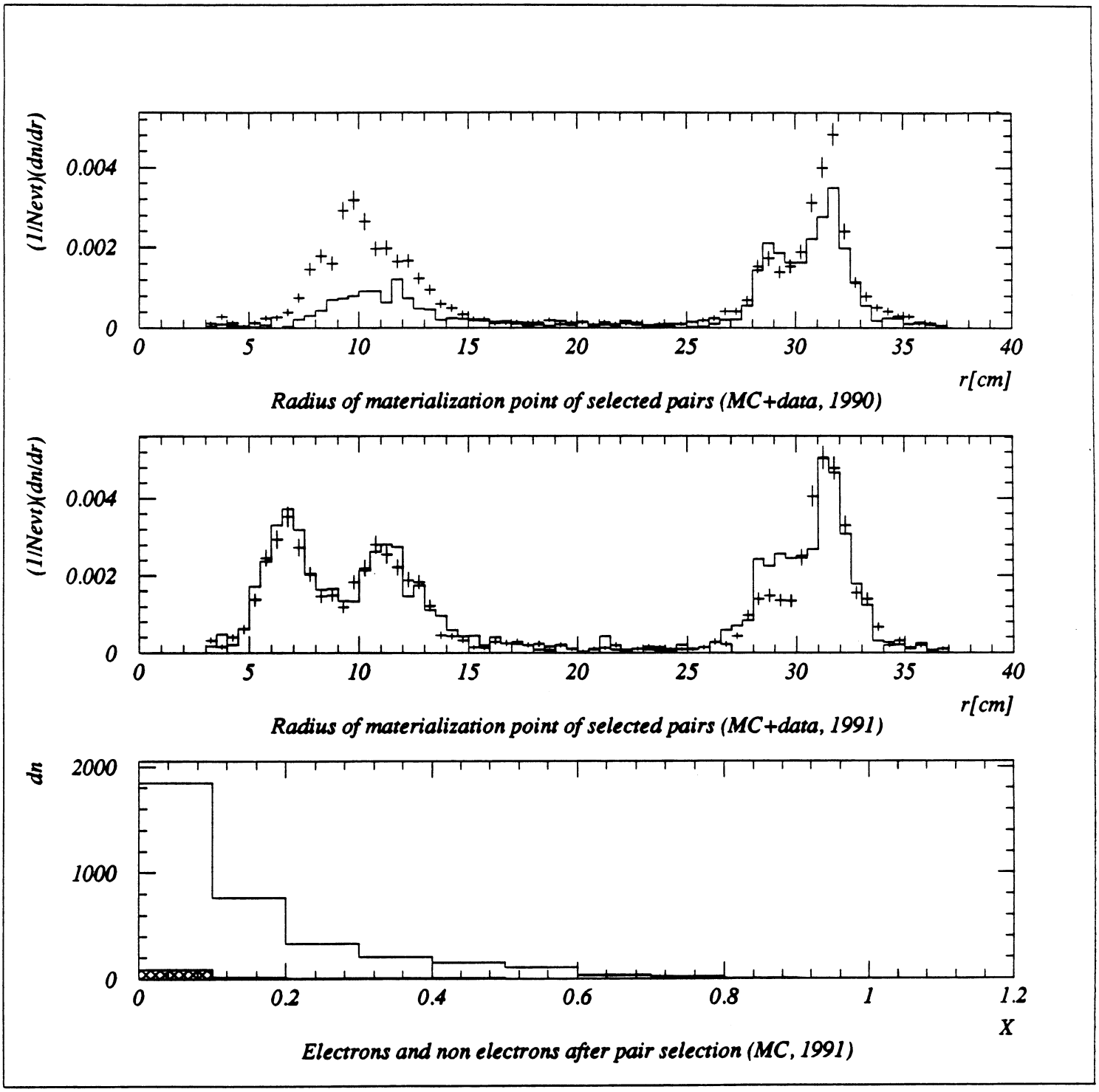

Figure 6 : The efficiency of the ECAL cuts (R2,R3) as a function of the pad energy measured with the electron test sample from conversion pairs and Bhabha events. The data is the points with the error bars, the MC is the histogram. The second plot shows the straight line fit to the ratio of both efficiencies. The first and the last bin are not included in this fit. The error bars between 0.8 and 1.0 are enlarged in order not to be biased by the incorrect momentum distribution in the 1990 Bhabha MC.

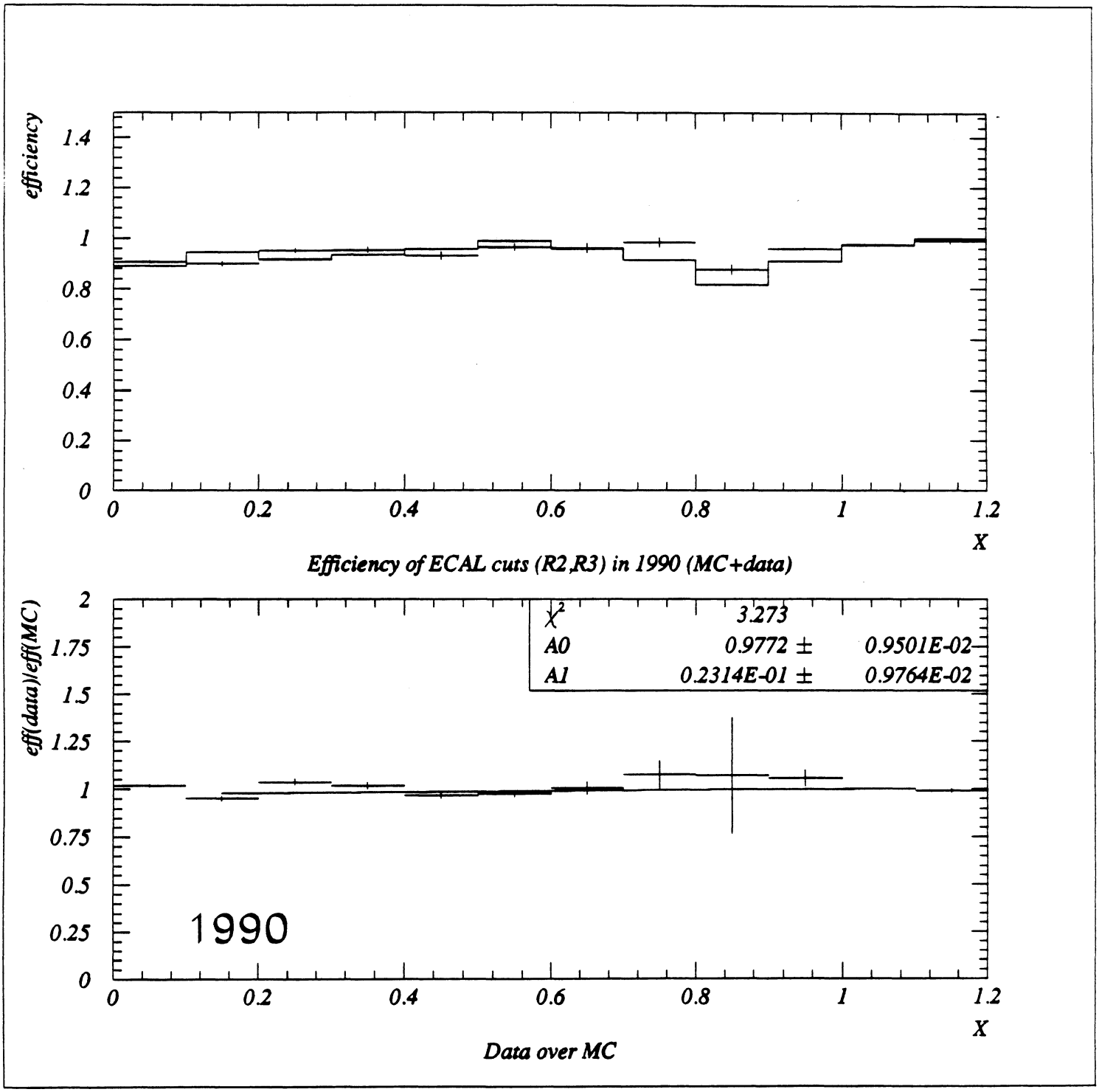

Figure 7 : The efficiency of the ECAL cuts (R2,R3) as a function of the pad energy measured with the electron test sample from conversion pairs and Bhabha events. The data is the points with the error bars, the MC is the histogram. The second plot shows the straight line fit to the ratio of both efficiencies. The first and the last bin are not included in this fit.

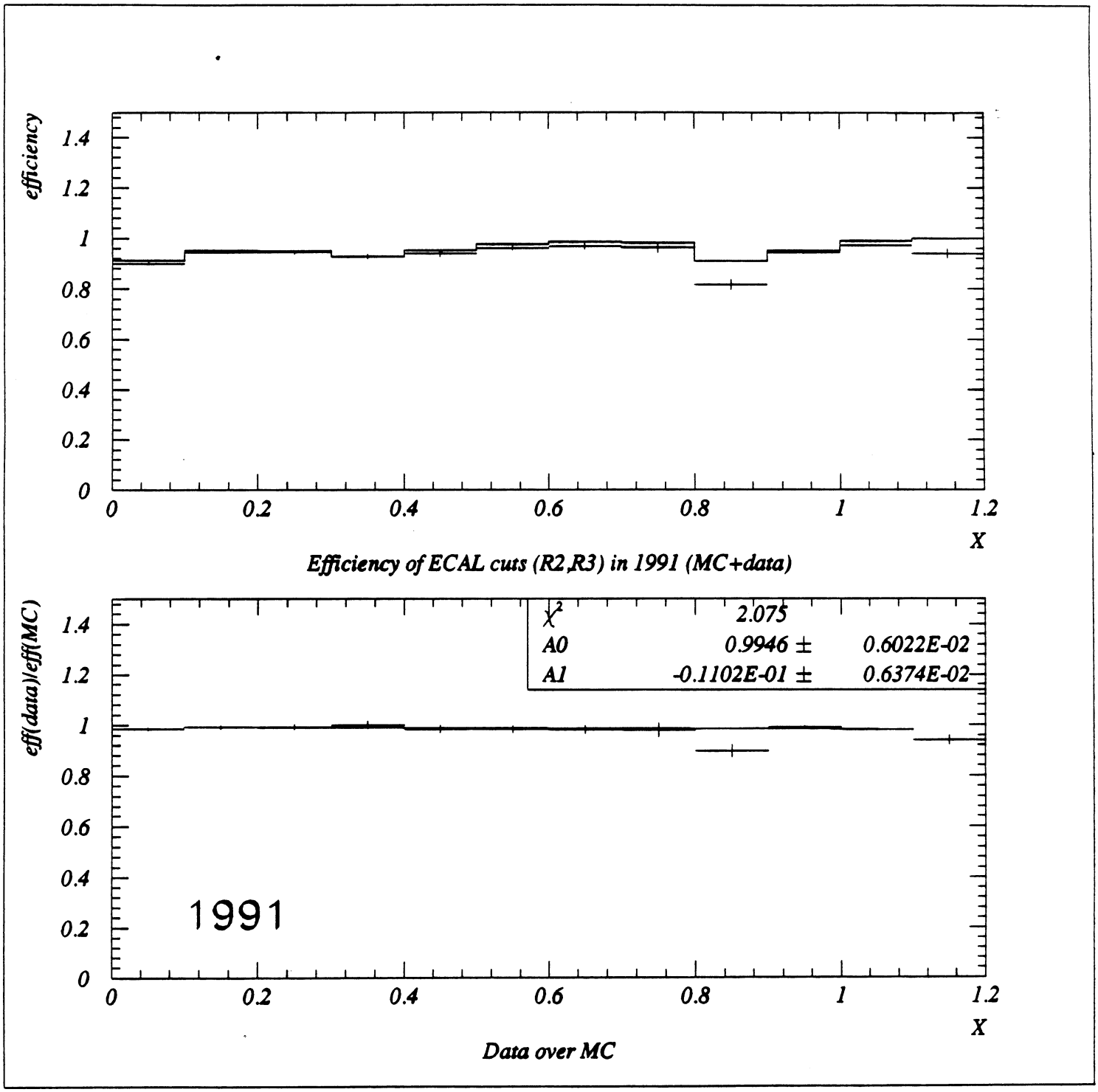

Figure 8 : The distribution of $X = p_{TPC}/E_{beam}$ for on peak Bhabha events. The data is the points with the error bars, the MC is the histogram. The striking discrepancy in 1990 is supposed to be due to the Bhabha generator giving too few photons.

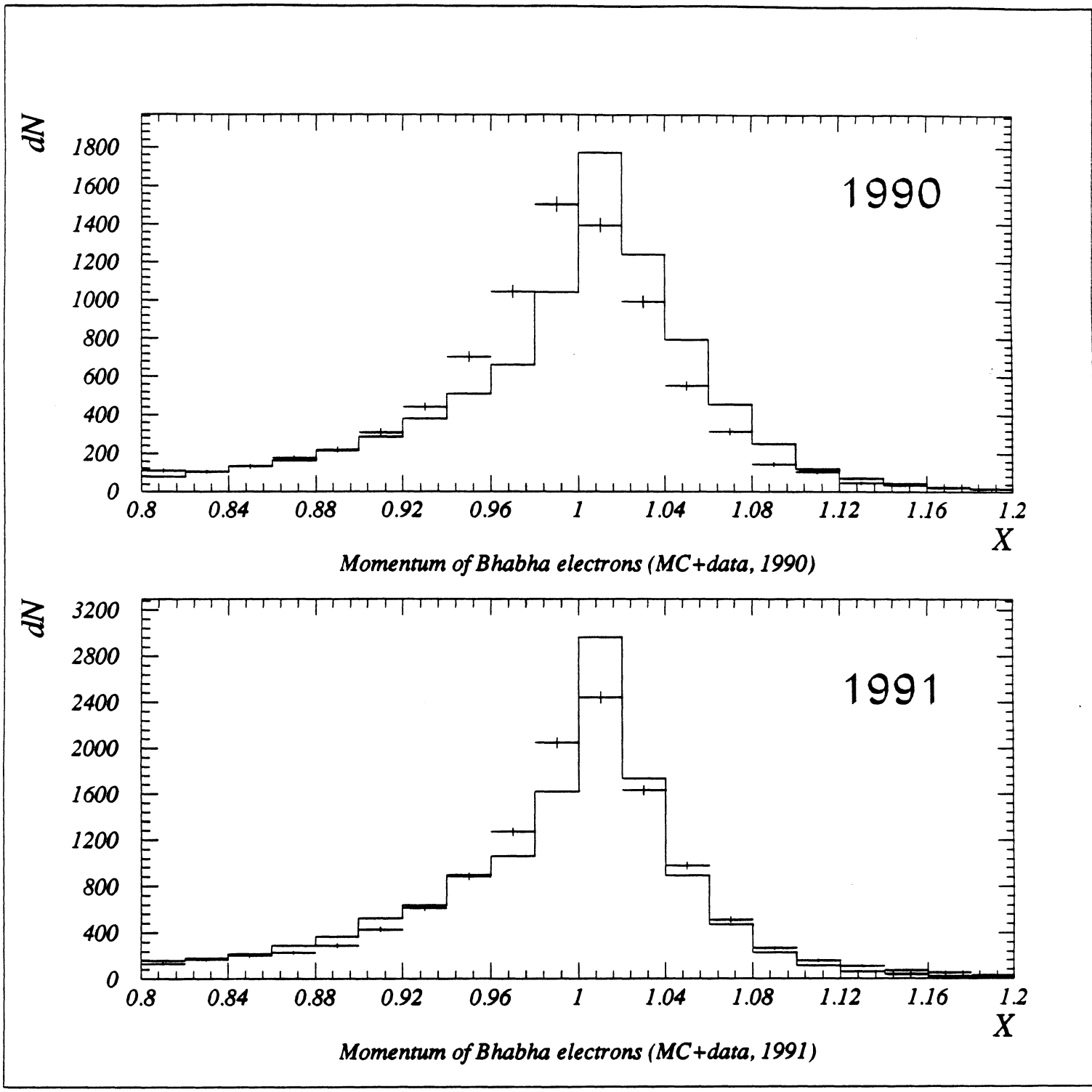

Figure 9 : The influence of the shift in the momentum distributions in the 1990 Bhabha test sample: the discrepancy between data and MC exists on both sides of the energy peak. But in the high X part ($X = E_{pad}/E_{beam}$) its influence on the efficiency of the cut $R2 > -2.5$ is negligible compared to the low X part.

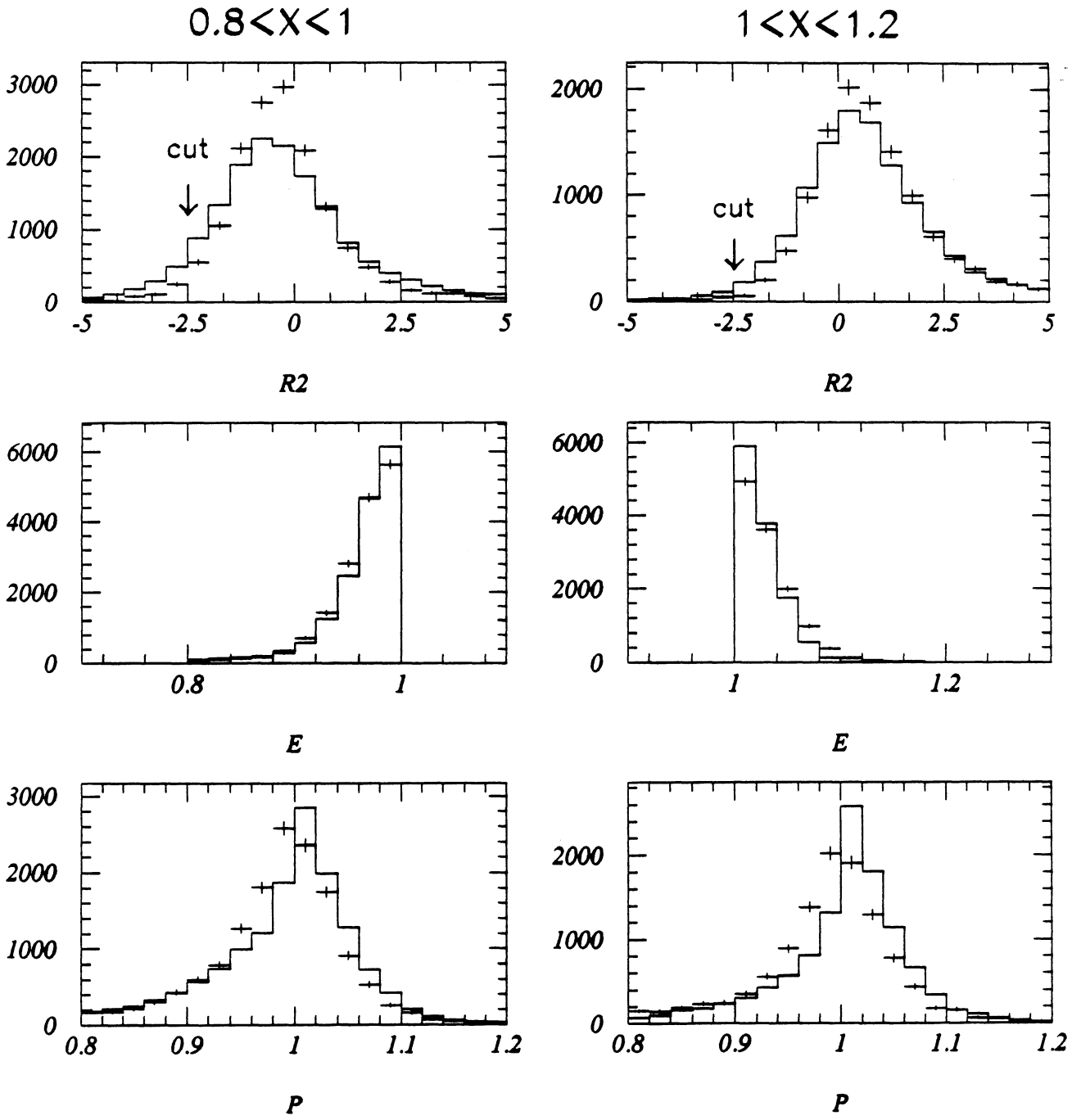

Figure 10 : The distributions of the dE/dx estimator for selected electron candidates in data and MC after all cuts.

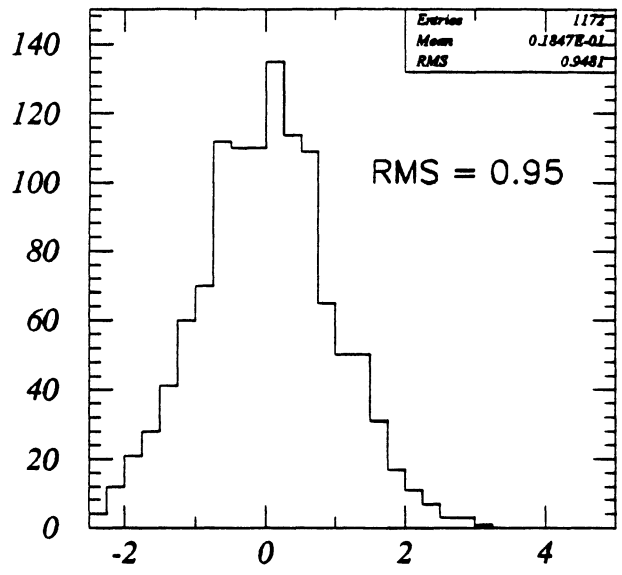

dE/dx estimator (data, 1990)

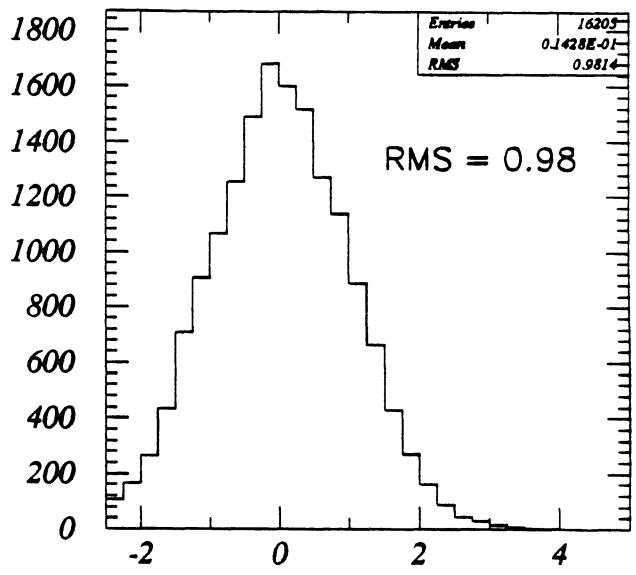

dE/dx estimator (MC, 1990)

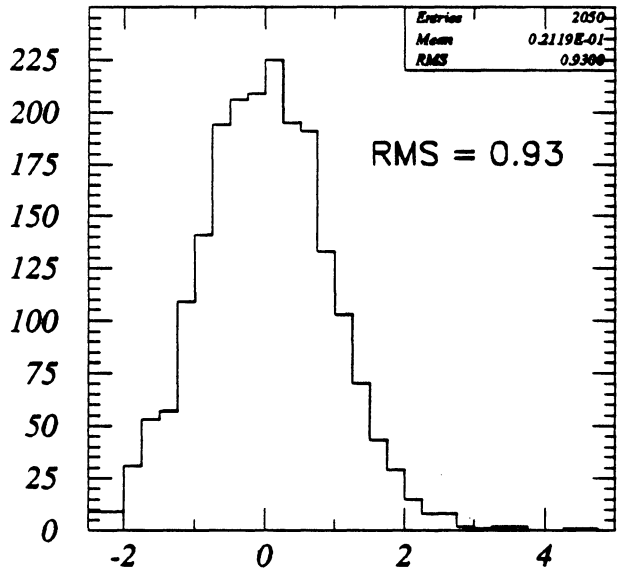

dE/dx estimator (data, 1991)

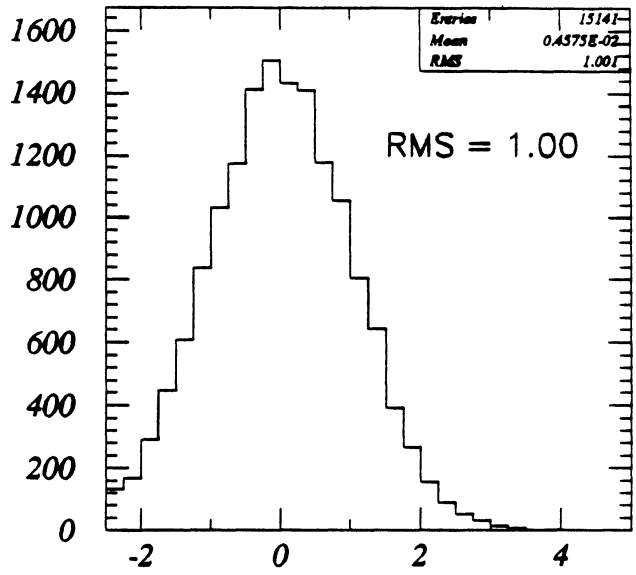

dE/dx estimator (MC, 1991)

Figure 11 : The distributions of the dE/dx estimator in 1990 before the cut at -2.5 was made. The MC has been devided into electrons (plain) and background (shaded). The relative normalization of both distributions is fitted to the data (points with error bars). The shaded part above -2.5 is the remaining background.

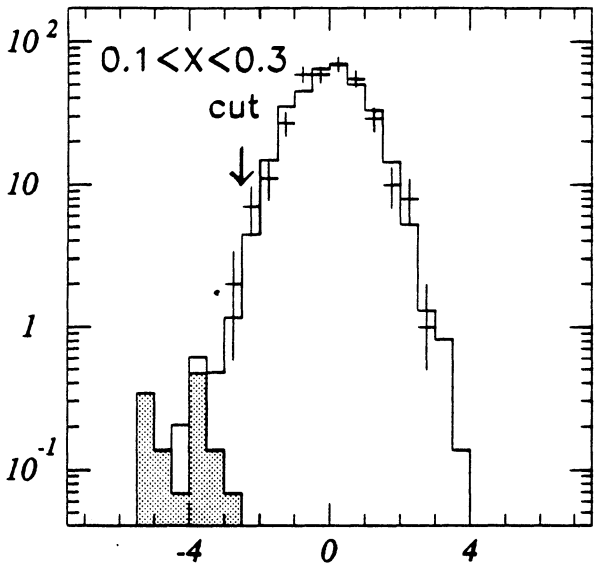

dE/dx estimator (1990), 1st energy bin

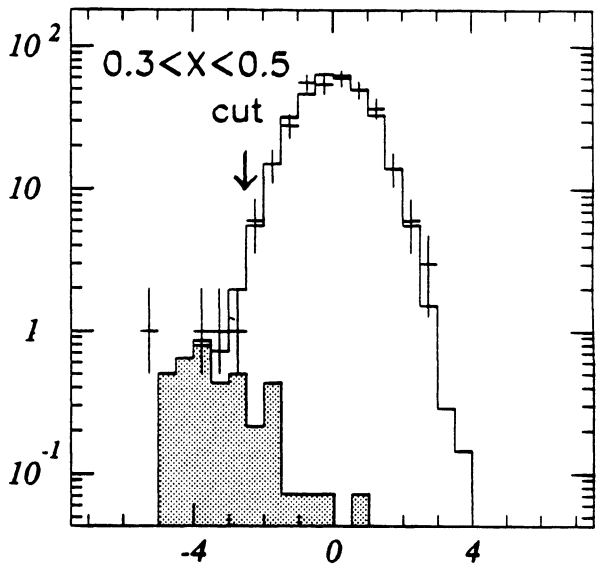

dE/dx estimator (1990), 2nd energy bin

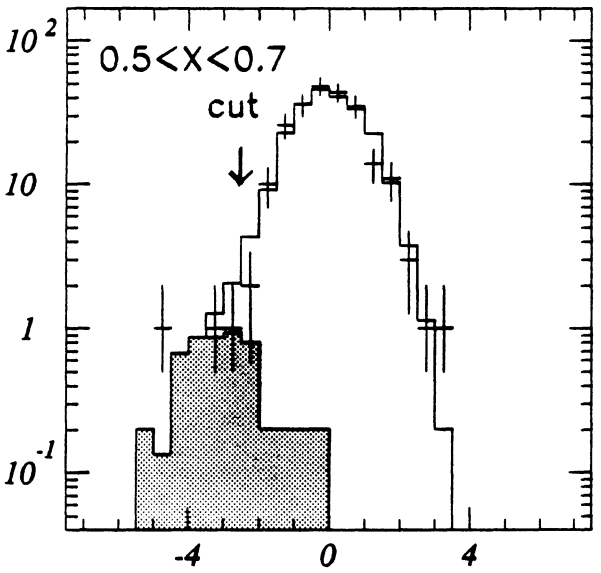

dE/dx estimator (1990), 3rd energy bin

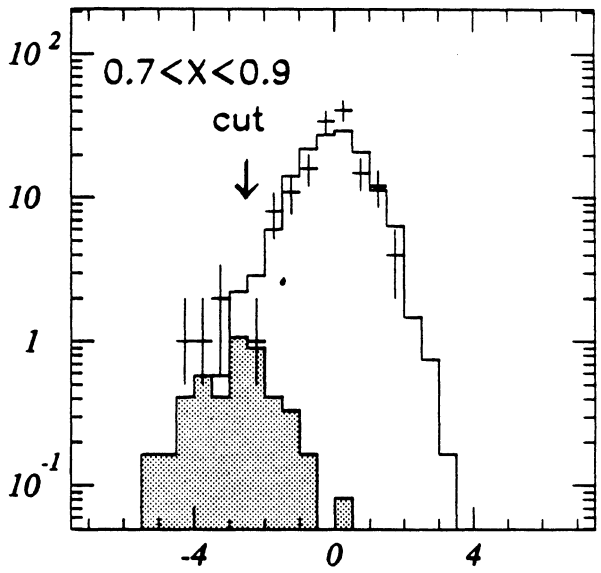

dE/dx estimator (1990), 4th energy bin

Figure 12 : The distributions of the dE/dx estimator in 1991 before the cut at -2.5 was made. The MC has been devided into electrons (plain) and background (shaded). The relative normalization of both distributions is fitted to the data (points with error bars). The shaded part above -2.5 is the remaining background.

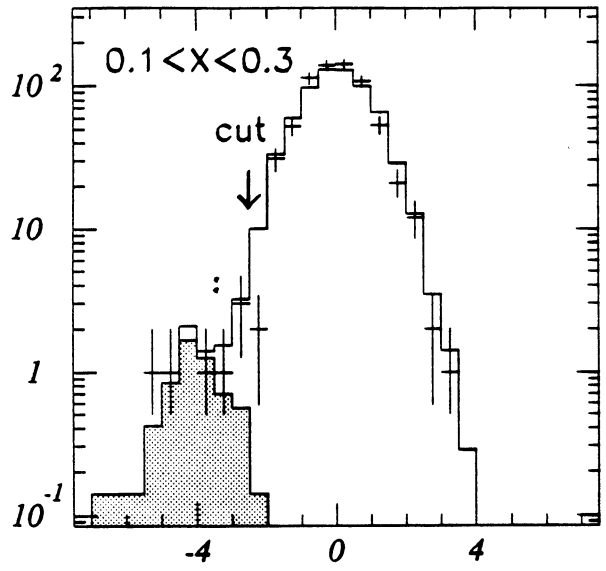

dE/dx estimator (1991), 1st energy bin

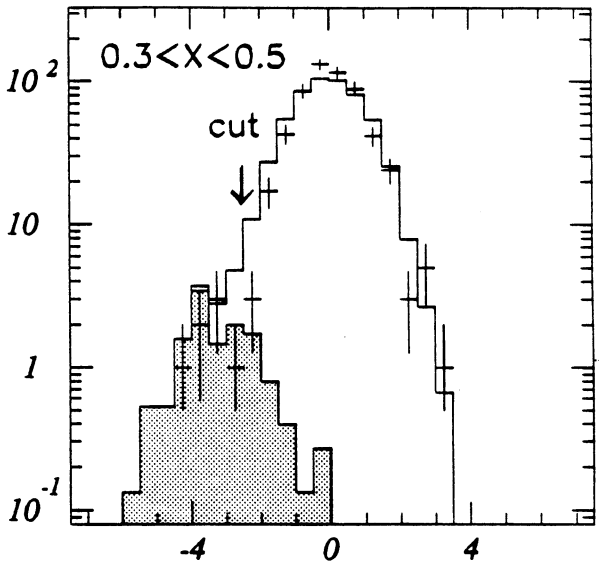

dE/dx estimator (1991), 2nd energy bin

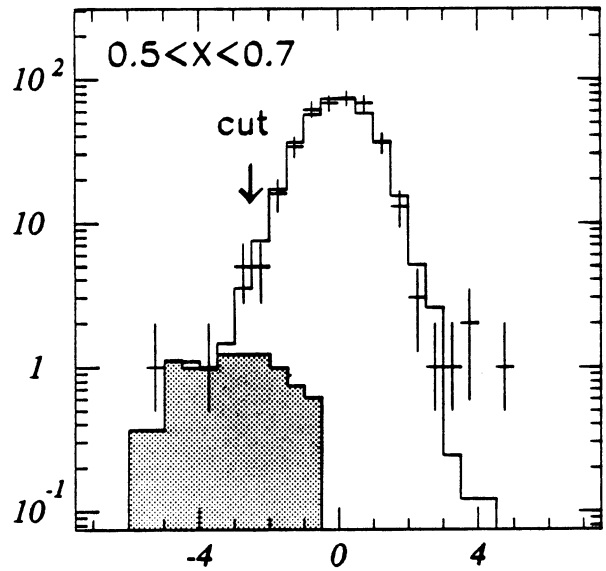

dE/dx estimator (1991), 3rd energy bin

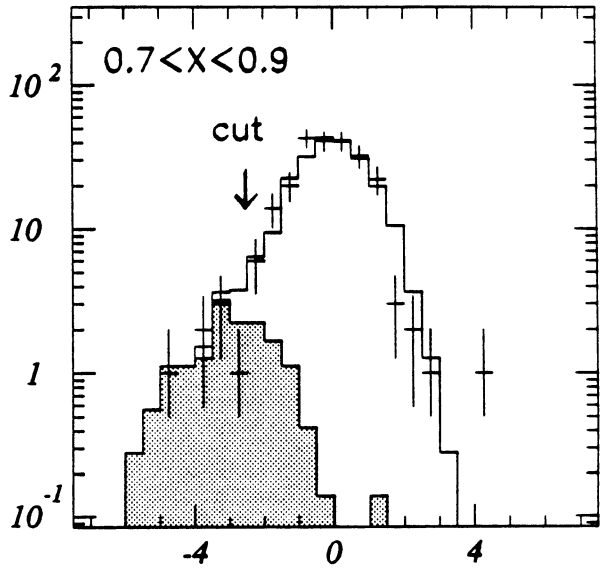

dE/dx estimator (1991), 4th energy bin

Figure 13 : The tau background in the fit region as a function of energy. The method to fit the distributions of the dE/dx estimator to the data is compared with the direct prediction of the MC.

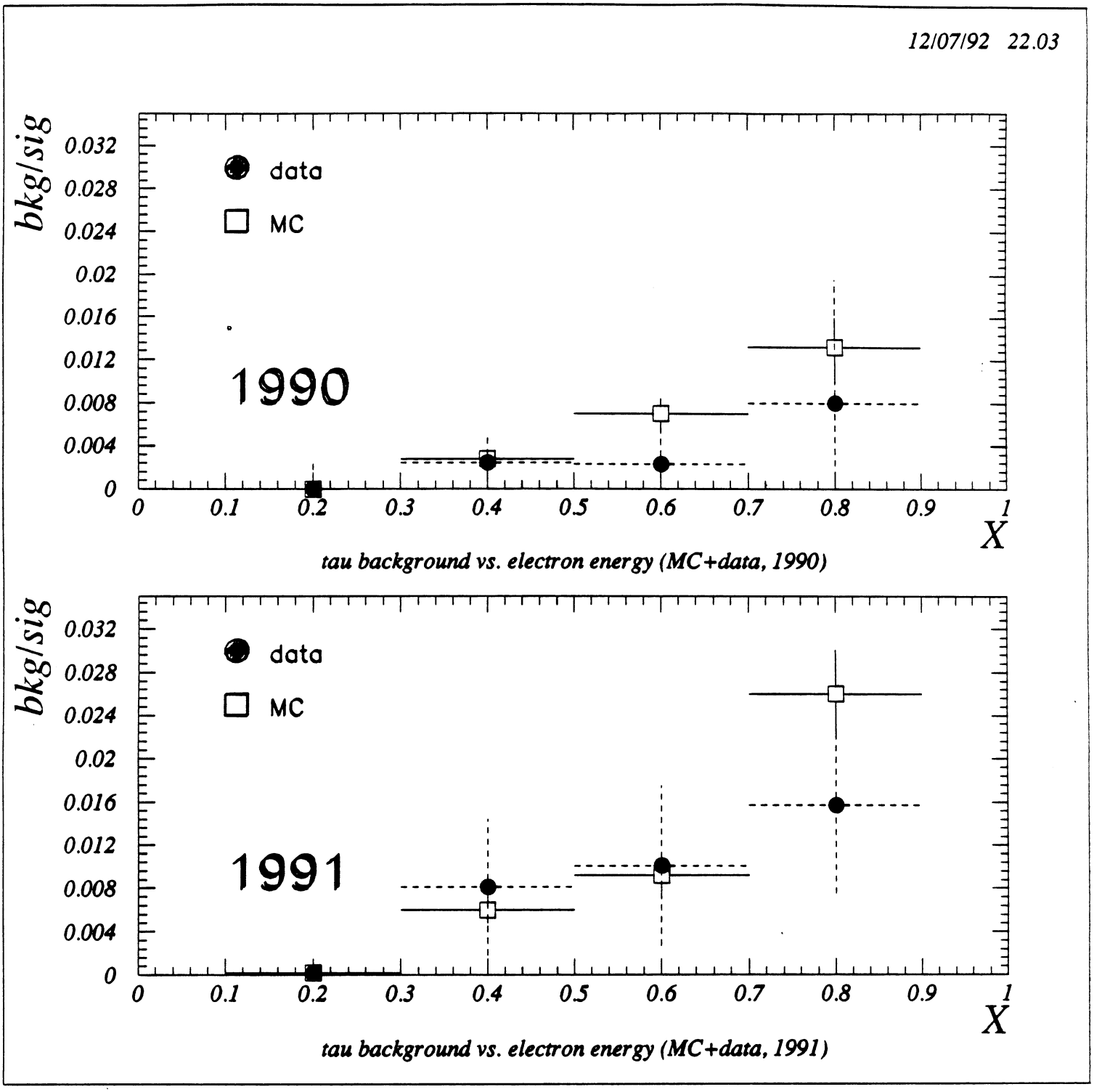

Figure 14 : The data spectrum of events with one identified electron in each hemisphere.

Figure 15 : The data spectrum of two electron events with more than 75% of the beam energy in the recoil hemisphere.

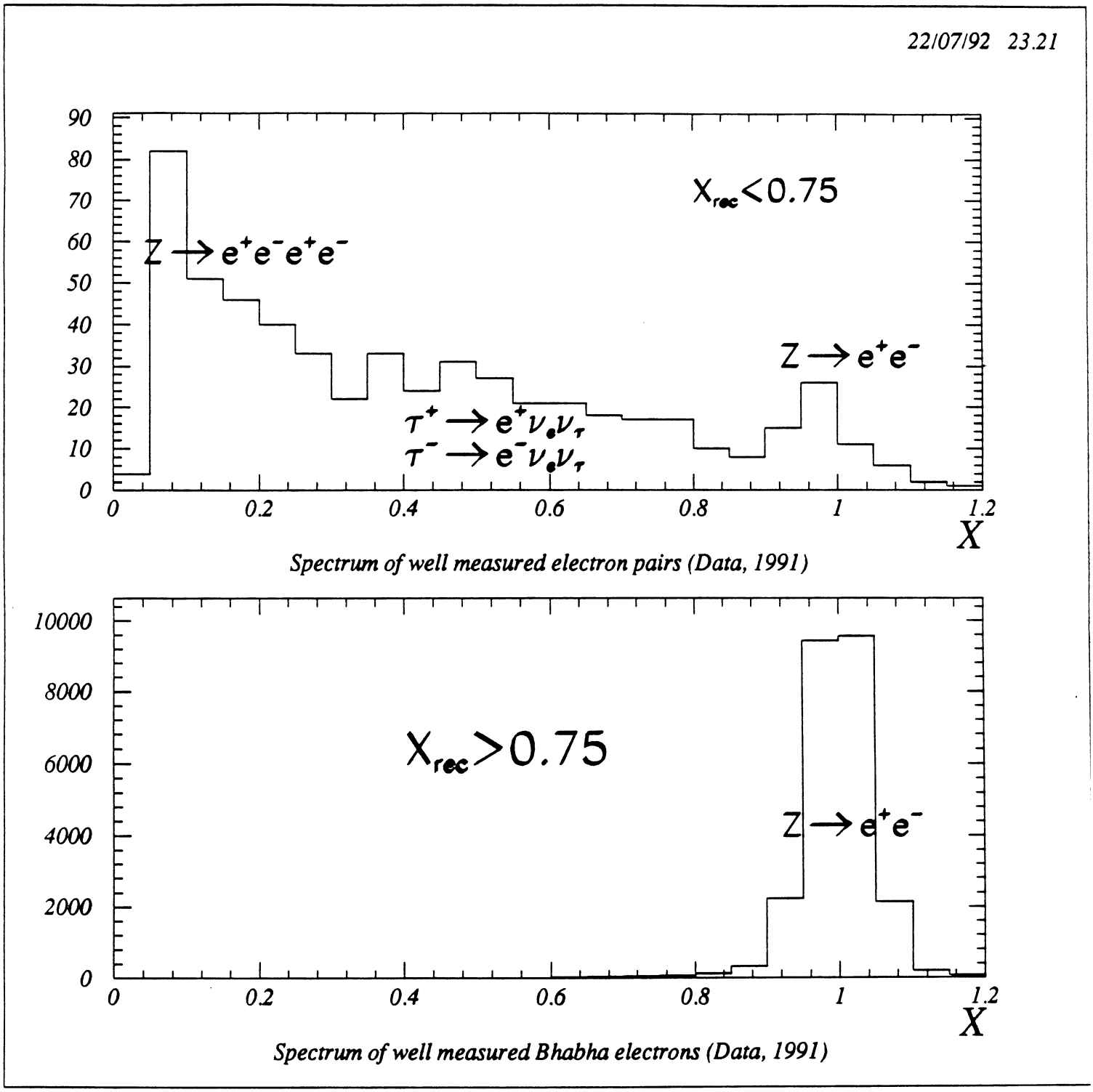

Figure 16 : The calibration of $X = E_{pad}/E_{beam}$ with on peak Bhabha electrons. The histograms are MC, the points with error bars are real data. There has been one calibration for the barrel and one calibration for both endcaps together. The mean of all distributions is centered at 1.000. Due to high Bhabha statistics the uncertainty of the mean is much less (about one order of magnitude) than the assumed uncertainty of the ECAL energy scale ($\pm 0.5\%$).

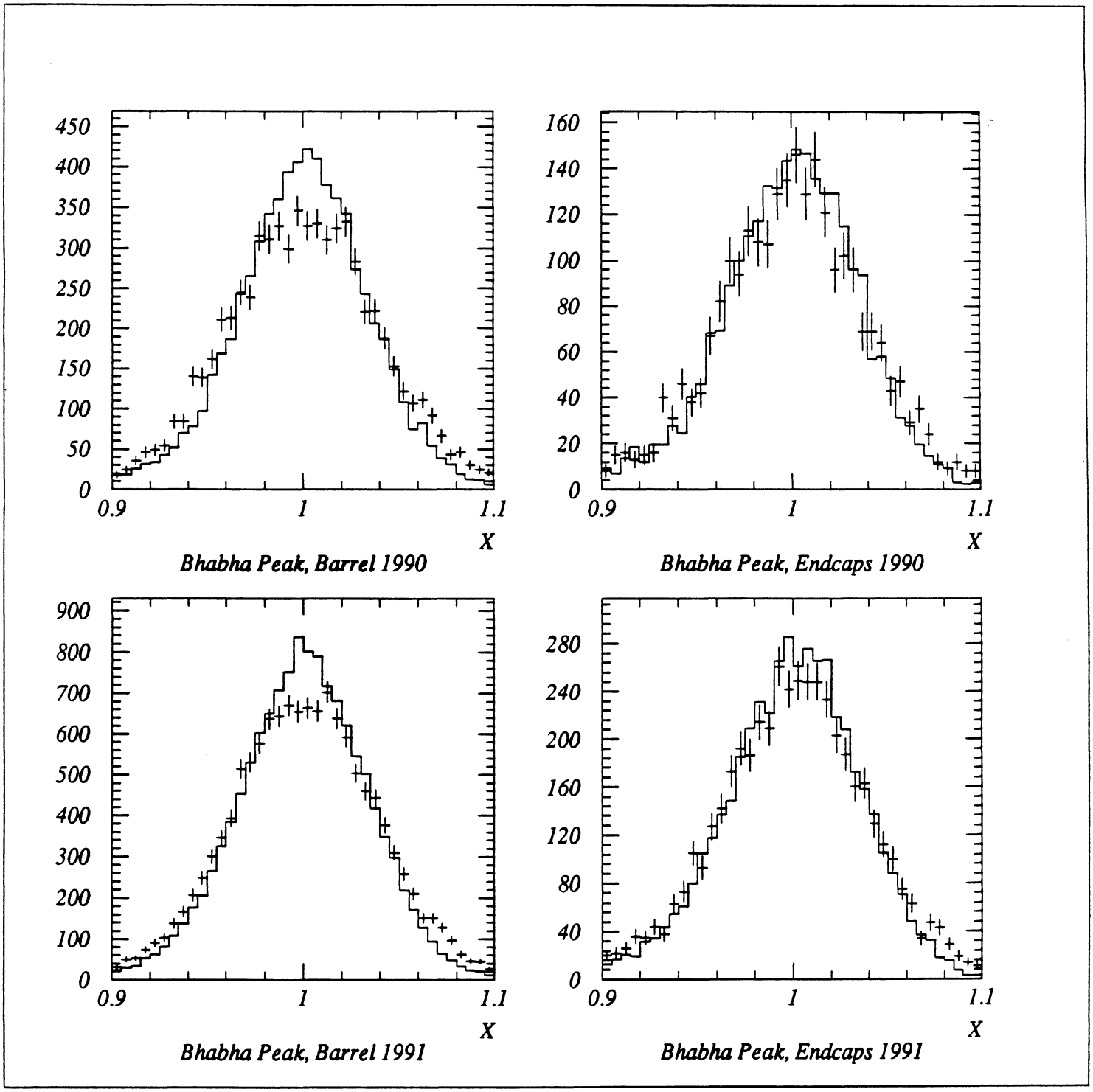

Figure 17 : The 1 parameter fit of $P(cos\theta)$ to the polarizations measured in the different $cos\theta$ bins.